Image Quality Issues

10

David Carmichael

1 fMRI Pulse Sequences

The requirement of a fMRI pulse sequence is BOLD sensitivity, which means predominantly T2*-weighted[1] sequences such as GE-EPI, although spin echo sequences such as spin echo EPI (SE-EPI) can also be used (Bandettini et al. 1994; Norris et al. 2002; Schmidt et al. 2005).

SE-EPI suffers from reduced volume coverage relative to GE-EPI due to the longer echo times required, and generally shows smaller signal changes (Bandettini et al. 1994; Schmidt et al. 2005). However, spin echo sequences do not suffer from signal dropout and therefore perform much better in areas of large through-plane susceptibility gradients (Norris et al. 2002). There is mixed opinion as to whether, or in which parts of the brain, spin echo sequences may be advantageous (Parkes et al. 2005; Schmidt et al. 2005), but they are likely to be most usefully employed at field strengths of >3 T (Duong et al. 2002; Nair and Duong 2004). Some considerable research has recently been devoted to using steady-state free-precession sequences for fMRI (Miller et al. 2003, 2004, 2006; Zhong et al. 2007). While these sequences have shown promise, they are generally employed for niche applications (Miller et al. 2006). It is also worth noting that hybrid approaches using spin and gradient echoes such as GRASE (Feinberg et al. 1995; Fernandez-Seara et al. 2005) are also capable of being used to obtain high-quality fMRI data.

[1]The transverse relaxation time including a contribution from slowly changing or constant background magnetic fields.

D. Carmichael
Institute of Neurology, University College London, Queen Square, London WC1N 3BG, UK
e-mail: d.carmichael@ion.ucl.ac.uk

C. Mulert and L. Lemieux (eds.), *EEG- fMRI*
DOI: 10.1007/978-3-540-87919-0_10, © Springer Verlag Berlin Heidelberg 2010

2 GE-EPI

The sequence of choice for most fMRI applications is GE-EPI, due to its high speed and a high signal-to-noise ratio (SNR) per unit time. An image can typically be obtained in 20–50 ms using modern hardware, giving whole brain coverage in 2–4 s (Schmitt et al. 1998; Mansfield 1977; Ordidge 1999; Turner and Ordidge 2000).

In the following section, we will restrict our discussion to Cartesian k-space trajectory EPI because it is the most frequently used and generally offers highly competitive performance in terms of speed and artefact level. Other k-space trajectories commonly used for EPI include spirals where both read and phase-encoding gradients are equivalent in pulse shape and amplitude, but offset in phase and oscillate in a sinusoidal manner (Ahn et al. 1986; Glover and Law 2001; Preston et al. 2004; Sangill et al. 2006). This can reduce image distortion, for example, due to faster traversal of k-space (especially compared to the phase-encoding direction of Cartesian EPI), but may not necessarily yield an overall increase in performance over the whole brain (Block and Frahm 2005).

An EPI sequence diagram is shown in Fig. 1. A gradient echo is formed when the transverse magnetisation is dephased and then rephased by linear magnetic field gradients alone (unlike a spin echo). The EPI experiment involves a single RF excitation pulse followed by a train of these echoes that are read out by applying a series of gradients with equal areas and opposite magnitude. Each echo has a different net phase-encoding gradient due to the extra gradients (blips) applied between the readout gradient reversals (Wielopolski et al. 1998). In EPI, all of the PE steps are acquired in one TR, making it a fast technique. This implementation of EPI is termed "single shot" because it requires only one RF excitation of the magnetisation to obtain an entire image dataset.

The echo time (TE) is centred on the middle PE step, where the net phase-encoding gradient is zero. It is clear that as each echo is at a different position in time, the magnetisation will have experienced different amounts of dephasing from any local magnetic field differences. These are caused by interfaces between materials of different magnetic susceptibility, such as the head and air. Any inconsistency between successive echoes, obtained at different times, has associated problems that will be discussed at greater length later. EPI can suffer from a number of other problems that are directly related to its strategy of full k-space coverage in a single shot. EPI readouts are naturally longer than for other pulse sequences, because a greater distance through k-space must be travelled in one go (see Fig. 1). Additional problems are associated with having reversed the direction travelled through k-space in alternate lines (see Schmitt et al. 1998 for an additional description of EPI artefacts and their causes). Here, we first look to explain the most common sources of EPI artefact in a qualitative manner, and we describe the range of methods available to moderate their effects before going on to determine how the addition of EEG equipment may exacerbate these image quality issues.

2.1 Image Blurring

Blurring of image detail occurs because of T2*/T2-related signal decay over the length of the acquisition (i.e. not all points in k-space are sampled at the same effective TE). For EPI,

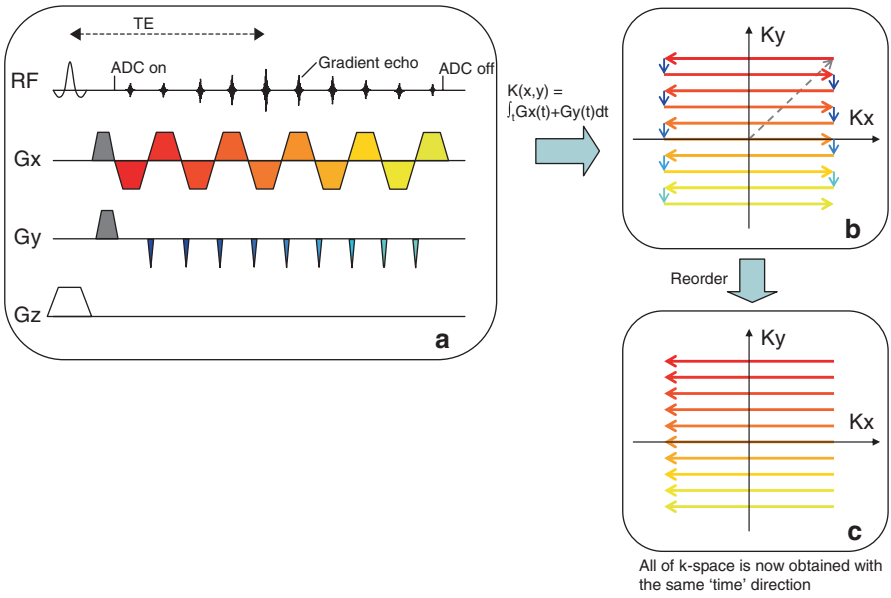

Fig. 1a–c Standard blipped Cartesian EPI pulse sequence and corresponding k-space trajectory. The blipped EPI pulse sequence is shown (**a**). On the *top line* is the RF showing the slice-selective excitation pulse followed by a series of gradient echoes. Each of the gradient echoes is formed by a readout gradient of opposite polarity. Additionally, for each gradient reversal a different phase encode line is readout by the application of a phase-encoding gradient during the read gradient reversal. ADC is the analogue-to-digital converter that is switched on to record the signal. **b** The k-space trajectory is shown; the position in k-space is determined by the gradient area. The colour of the gradient corresponds to the k-space trajectory. Initially, the *grey* gradients take us to the k-space corner, and then the readout gradient alternately traverses from *right* to *left* while the phase-encoding blips make the jumps from *top* to *bottom* at the end of each readout gradient. It is worth noting that the order that k-space is acquired in the phase-encoding direction can be reversed (here the blips are negative), and this will alter the distortion (see Fig. 3 and consider the effect on the k-space trajectory of opposite-sign phase-encoding blips). **c** Alternate lines of data are reversed in direction prior to reconstruction. This effectively means that each line of k-space data should look as if it has been obtained under the same polarity of gradient (otherwise each line appears as if time was reversed). Any mismatch between positive and negative gradients creates a mismatch along the K*y* direction in alternate lines and causes an N/2 ghost

the large time difference between adjacent k-space data points, particularly in the phase-encoding direction, causes greater signal decay and thus increased blurring. This can be thought of as the effective application of a filter in k-space described by the signal decay during the readout with the blurring caused in the image described by the Fourier transform of this filter, which is called the point spread function (PSF) (see Fig. 2). In tissue with a shorter T2*, due to stronger local susceptibility-related magnetic fields that are increased by utilising higher main magnetic field strengths, this problem is increased. Blurring will thus also be increased where stronger local susceptibility-related magnetic fields are produced by EEG equipment. Reduced blurring is achieved by shorter readout lengths or higher resolution images without increased readout duration. Methods to shorten readouts include multishot segmented EPI (Menon et al. 1997; Wielopolski et al. 1998), related

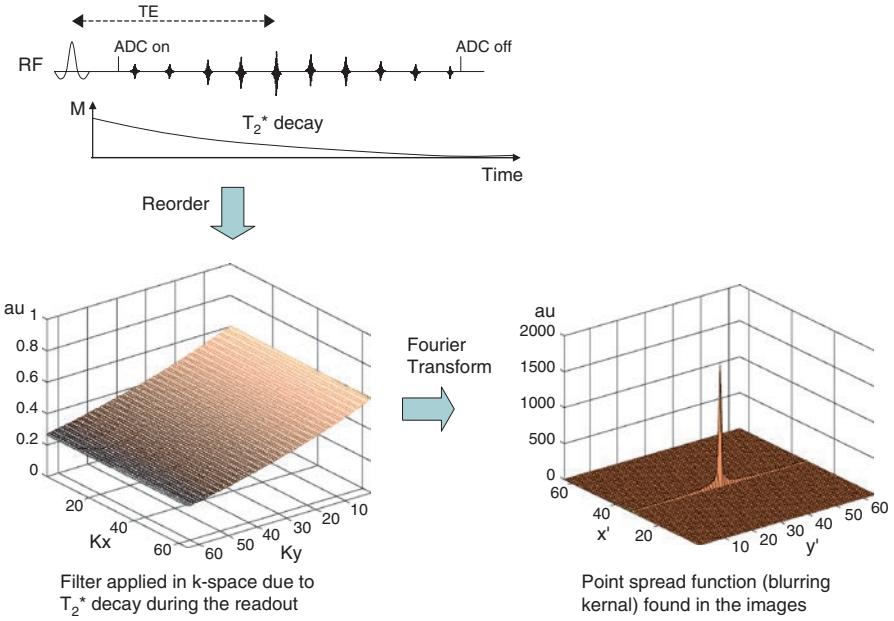

Fig. 2 Blurring in EPI images. Due to the properties of the Fourier transform we can separately consider each of the different components that modulate the underlying k-space signal produced by an object (that are all multiplied together in actual data). Each of these components can be thought of as a filter. The effect seen in the image is blurring from a convolution of the object by the Fourier transform of each k-space filter. There is a large amount of signal decay during the long EPI read out (*top*), which can thus be considered independently of other signal modulations (e.g. those imposed by imaging gradients or the object itself). When the data is reordered in k-space, the signal decay makes a 2D function in k-space that is an effective filter, as shown *bottom left*. The Fourier transform of this filter determines the point spread function, which describes the blurring of the data from each voxel

pulse sequences that split the readout into shorter segments without requiring multishots (Bornert and Jensen 1994; Carmichael et al. 2005; Feinberg et al. 2002; Priest et al. 2004; Rzedzian 1987) and parallel imaging (PI) methods (Carlson and Minemura 1993; Griswold et al. 2002; Hutchinson and Raff 1988; Pruessmann et al. 1999; Sodickson and Manning 1997). Alternatively, improved shimming (Cusack et al. 2005; Gruetter 1993; Gruetter and Tkac 2000; Mackenzie et al. 1987; van Gelderen et al. 2007; Ward et al. 2002; Wilson et al. 2003; Wilson and Jezzard 2003) can also locally decrease blurring by increasing local field homogeneity. In most fMRI experiments, including EEG–fMRI, blurring is not a primary consideration for pulse sequence optimisation. This is due to the usual spatial extent of activation exceeding the voxel size and because the optimisation of SNR, temporal resolution and image dropout is usually more critical. However, it is important to remember that the resolution is degraded, especially in the phase-encoding direction in GE-EPI, and in some cases where small structures are interrogated—such as high-resolution mapping of cortical columns within visual areas—some minimisation of blurring may be beneficial.

2.2 Geometric Distortion

Due to the time difference between the acquisition of adjacent k-space data points in the phase-encoding direction (or correspondingly the low (PE) bandwidth, which is simply the reciprocal), local magnetic field perturbations from various sources (Jezzard and Clare 1999; Wielopolski et al. 1998) have the time to cause significant local phase accumulation relative to that produced by the phase-encoding gradients (i.e. the local magnetic field gradient area is large relative to the size of the phase-encoding blips). This causes an apparent shift in the data from the local position in the image, with the shift in position proportional to the size of the local difference in the local static magnetic field (B_0) (Jezzard and Balaban 1995). In addition to a simple shift of data from one position to another, data from one position may be stretched over a larger area or squashed into a smaller area. In Fig. 3, the process is described in terms of k-space coverage. At different positions within the brain, there is a local magnetic field gradient that has an additive effect, positive or negative, on the phase-encoding gradients. This can be conceptualised as causing a different k-space trajectory for magnetisation at a different spatial position. In one spatial position, the phase encoding (Ky) covers a greater effective k-space area and the lines are further apart. This corresponds to squeezing the data into a smaller area. Alternatively, the lines are forced closer together, with the effect of stretching the data in the image. Distortion will be increased where stronger local susceptibility-related magnetic fields are produced by EEG equipment.

The simplest method of reducing distortion is to shorten the time between the phase-encoding blips by switching the read gradients faster and with greater amplitude, thereby requiring an increased readout bandwidth (with a concomitant reduction in SNR). This corresponds to reducing the time taken to travel through the k-space trajectory in Fig. 1. Unfortunately, the rate and maximum amplitude of the read gradient switching is limited by physiological constraints; rapidly varying magnetic fields can induce currents in nerves large enough to cause stimulation (Cohen et al. 1990; Mansfield and Harvey 1993). In addition, the desired gradient waveform is only accurately produced when both its amplitude and switching rate lie within certain limits. Therefore, one option that is available is to reduce the number and increase the size of the phase-encoding steps in the acquisition window, necessitating the recovery of a full set of image information by some other means. There are a number of different techniques that are used to perform this function, and they can be classified into two approaches. First, there is interleaved segmented EPI (Butts et al. 1994; Hennel and Nedelec 1995) (for two segments, every other line of the standard k-space coverage is read out, and then the remaining lines are read out in a separate acquisition), although this entails a penalty in temporal resolution that would be unacceptable for many fMRI applications. Various strategies have been suggested to read out the segments consecutively. One of the simplest is to use a 45° RF pulse and acquisition followed directly by a 90° RF pulse and acquisition (Rzedzian 1987), or to take pairs of images with different spatial profiles imposed and then reconstruct the data (Carmichael et al. 2005; Feinberg et al. 2002; Priest et al. 2004). The second approach uses differing degrees of prior information to recreate full images from reduced data sets. Partial Fourier methods that exploit the conjugate symmetry of k-space have been used (Feinberg et al. 1986), but

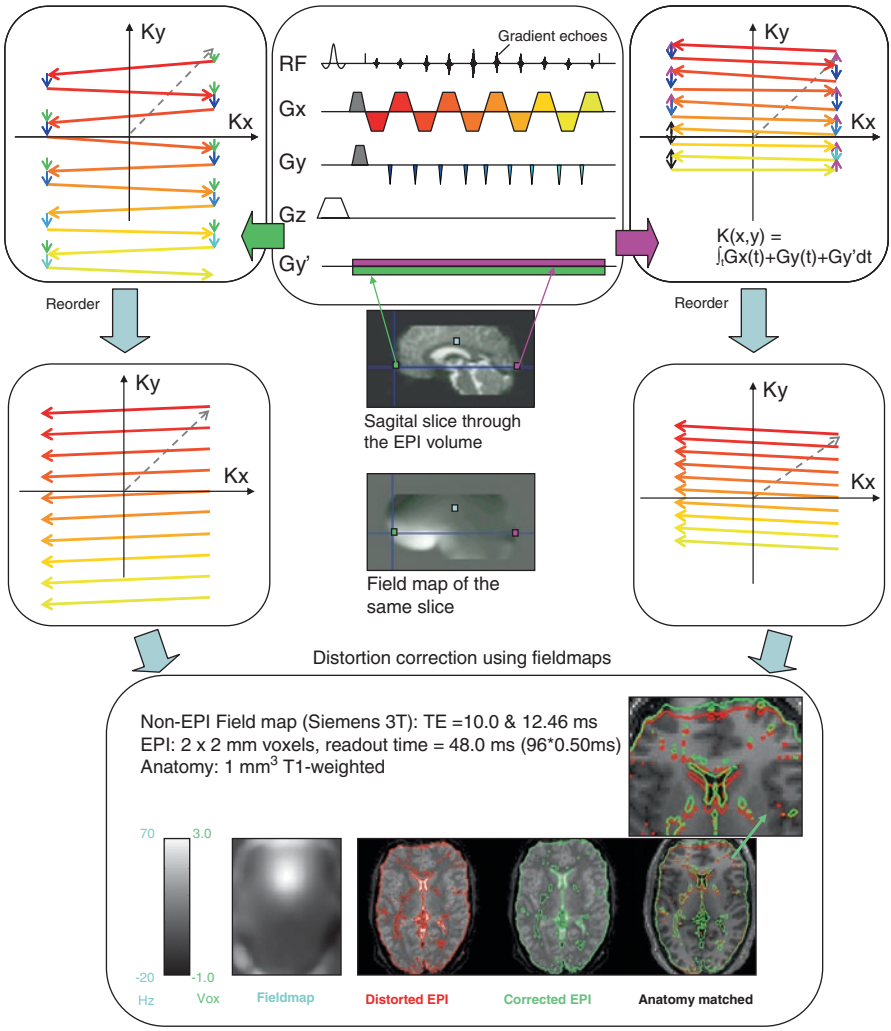

Fig. 3 Distortion in EPI images. When an extra local in-plane gradient is present in the phase-encoding direction due to susceptibility artefacts, the effective local k-space trajectory is altered. If the local gradient adds to the PE blips (as on the *left*), then the distance between the lines and k-space area covered is increased and this will cause the data to be spread over a larger area. This will make the local image data appear stretched. Alternatively, if local gradients have opposite polarity to the PE blips (as on the *right*), the k-space trajectory has less distance between the lines and covers a smaller area, and so the local image data will appear squashed. Fieldmap-based distortion correction is shown at the *bottom*. The fieldmap was obtained using a standard gradient echo sequence and two complex images at different echo times, which were masked, phase unwrapped and smoothed. This can be converted into units of displacement (here in voxels), and then the EPI image can be unwarped using the voxel displacement. This improves the match to the anatomical image that does not suffer from distortion

they do not always significantly reduce distortion and can introduce increased blurring. In recent years, a new group of methods, collectively known as parallel imaging (PI) have allowed a considerable increase in acquisition speed (Carlson and Minemura 1993; Hutchinson and Raff 1988; Pruessmann et al. 1999; Sodickson and Manning 1997). These all rely on the parallel use of receiver coils with different spatially varying sensitivities. Some calibration of the sensitivity functions of these coils gives information that is complementary to standard Fourier encoding. This allows a reduction in the density with which k-space must be sampled, reducing the distortion by the factor of speed-up (reduction in sampling density) employed in the PE direction. The penalty for all of these methods is a reduction in SNR and a potential increase in image reconstruction artefacts that can outweigh the benefits (Lutcke et al. 2006). Lastly, there are methods for correcting the distortion. These rely on mapping the underlying B_0 field, which means that the distortion can be spatially calibrated and corrected. Methods for B_0 mapping are numerous (e.g. Gruetter and Tkac 2000; Lamberton et al. 2007; Mansfield 1984; Poser et al. 2006; Priest et al. 2006), but most simply perform two scans at different TEs. The local phase difference between the images is proportional to the local magnetic field. The phase difference can then be translated into a pixel shift map to visualise and correct these distortions, as shown in Fig. 3 (Chen and Wyrwicz 1999; Hutton et al. 2002; Jezzard and Balaban 1995; Munger et al. 2000; Reber et al. 1998; Schmithorst et al. 2001; Zaitsev et al. 2004). The main limitation of this method is that information from regions where the data is squashed into a smaller area cannot be fully recovered. This can be overcome if images are obtained with alternate directions for k-space traversal (in the PE direction), effectively switching the areas that are squashed to being stretched and vice versa (Morgan et al. 2004; Weiskopf et al. 2005). However, differences between alternate volumes can be hard to eliminate, and an effective reduction in temporal resolution or volume coverage is likely. Distortions can still pose a problem for standard fMRI and EEG–fMRI studies, particularly when high structural fidelity is required, such as when fMRI is used to assist in presurgical mapping of eloquent cortex, or where presurgical EEG–fMRI results from epilepsy patients are evaluated against structural images obtained postresection.

2.3 Signal Dropout

Dropout, like distortion, is due to strong local magnetic field gradients interfering with the image acquisition process. There are two related but distinct mechanisms by which signal dropout can occur. The primary mechanism is due to local fields across the slice (through the imaging plane). The local magnetic fields cause magnetisation at different positions across the slice width to produce signals with corresponding frequencies. These signals from different positions will, with time, accumulate differing phases and so cancel; the net effect is more rapid signal decay (see Fig. 4). If the signal decays substantially before the centre of k-space has been traversed, where the main low-frequency components of the signal are encoded, the majority of the signal is not sampled and so the region will appear dark. The second mechanism is dropout due to in-plane gradients; if the in-plane gradients are strong enough, they will alter the k-space trajectory (i.e. an

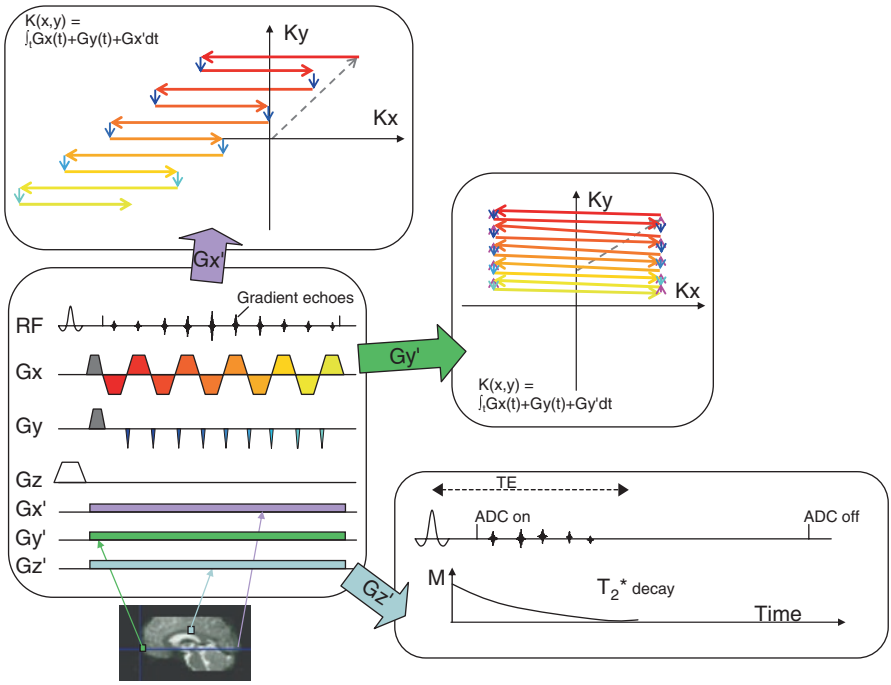

Fig. 4 Dropout in EPI images. Different mechanisms that cause signal dropout in EPI images are shown. An extra local gradient is present due to susceptibility artefacts (G*x*', G*y*' or G*z*'). In the case of a local gradient G*z*' from one particular position, this causes faster T_2* decay via through-plane dephasing, such that the signal has decayed before the centre of k-space has been sampled. Dropout can also occur when the local in-plane gradients G*x*' or G*y*' cause an alteration in the k-space trajectory such that the centre of k-space is not sampled. Note that even if the k-space centre is sampled, this will occur either much earlier or later in the echo train, leading to a greatly reduced BOLD sensitivity

extreme example of what we saw previously for distortion). For dropout to occur, the trajectory must be altered radically such that the central region of k-space is not covered (see Fig. 4) (Deichmann et al. 2002, 2003; Weiskopf et al. 2006, 2007). It must also be remembered that in-plane gradients are still problematic even when dropout does not occur. This is because the effective TE (the point at which the centre of k-space is sampled) is shifted in time to earlier or later in the readout. An earlier TE will mean that there is strong signal but little BOLD contrast, whereas a later TE will have strong contrast but the signal will have decayed too much. Both in-plane and through-plane local susceptibility-related gradients can be increased where stronger magnetic fields are produced by EEG equipment.

There are a number of approaches that can be adopted to minimise dropout, primarily concerned with through-slice effects. The first consideration is the TE; reducing the TE means that the centre of k-space will be covered sooner, before the signal has largely decayed, and so reduces dropout. However, the BOLD sensitivity is reduced with TE.

The balance required is to minimise the TE without strongly reducing the BOLD sensitivity (Deichmann et al. 2002). At 1.5 T, this means that a TE of around 50 ms is typically used, shortening to around 30 ms at 3 T. Another initial very simple approach is to decrease the slice thickness, reducing the frequency range across the slice, and hence the degree of phase dispersion that will occur (Frahm et al. 1993; Merboldt et al. 2000). Some penalty is incurred in terms of signal for well-shimmed areas (i.e. areas with a uniform local magnetic field) due to decreased voxel volume, whereas poorly shimmed areas will benefit from a large increase in signal. There is also a penalty in terms of volume coverage, although gaps between slices can be increased. The balance between these different factors will depend on the particular experiment, regions of primary interest, the sequence and the scanner. In addition to making the slices thinner, the orientation of the slices can also be altered to minimise dropout (Cho et al. 1988; Deichmann et al. 2002; Weiskopf et al. 2006). Since the primary loss is due to gradients across the slice, by changing the slice tilt the size of the local gradients perpendicular to the slice plane can be reduced. However, slice tilting is often used to reduce the size of in-plane gradients that are causing dropout or reduced BOLD sensitivity. The increased through-plane gradients are then compensated with a z-shim (discussed below).

Despite optimising TE, slice thickness and slice tilt, significant dropout can still occur, particularly in orbitofrontal regions and the temporal poles (Deichmann et al. 2003). The local B_0 gradients produced by putting a subject into the magnet field can be compensated for by using a pulse sequence with an additional preparatory gradient of opposite polarity but similar area, which is generally referred to as a z-shim (Constable and Spencer 1999; Frahm et al. 1988; Ordidge et al. 1994a). There are two main effects from utilising a z-shim. Firstly, in areas of the brain that are not affected by strong local gradients, the T_2* is effectively increased and so this can reduce the BOLD sensitivity when using the same TE sequence. This suggests that only a moderate z-shim can be used without a significant penalty in sensitivity over much of the brain (Deichmann et al. 2002). Secondly, in areas where the z-shim compensates for local gradients, a large improvement in dropout is achieved with a correspondingly large improvement in sensitivity to BOLD signal changes. Unfortunately, it is normally difficult to achieve a z-shim improvement in one area without a decrease of performance in another, and so the optimal choice of z-shim (and slice tilt combination) will depend on the regions of most interest for a particular study (Deichmann et al. 2002; Weiskopf et al. 2006, 2007). One way to achieve a more optimal z-shim for a greater range of areas is to use a multiecho EPI readout (Poser et al. 2006). This means that images can be obtained at several different TEs and with different compensation gradient polarities or directions. The images can then be combined very simply (e.g. by addition), or by a weighting scheme devised from calibrating BOLD sensitivity to maximise the benefits (Constable and Spencer 1999; Poser et al. 2006). There can be some cost in terms of the time taken to obtain the data from each slice, which in turn may reduce volume coverage, making a simple reduction in slice width an attractive and simpler choice. However, multiecho EPI sequences have a very high ratio of data acquisition time over scan time and so can offer a very efficient alternative strategy. Dropout is often the greatest problem in both fMRI and EEG–fMRI studies. Dropouts can be made worse (or at least BOLD sensitivity may be reduced) where EEG equipment produces increased magnetic field inhomogeneity within the brain.

2.4 Image Ghosting

In EPI, ghosting is normally produced by a mismatch between echoes formed by read gradients of opposite polarity. In Fig. 1, the process of reordering k-space is demonstrated; alternate lines are reversed (flipped about the origin) in order to have traversed k-space in the same direction for each line. Any inconsistency between lines acquired under positive- or negative-polarity gradients will cause an error in the image reconstruction (i.e. a flipped positive gradient line should be the same as a negative line if the phase encoding is the same). As alternate lines are affected, a ghost (a partial repeat of the image) will appear displaced in the phase-encoding direction by half the field of view. While this is often referred to as the "Nyquist ghost", this is misleading as it is not a data undersampling error but a mismatch between alternate PE k-space lines, and thus the term N/2 ghost is more accurate. Gradient inconsistencies, eddy currents and susceptibility gradients can all contribute to this mismatch (Feinberg and Oshio 1994; Fischer and Ladebeck 1998; Reeder et al. 1997; Wan et al. 1997; Wielopolski et al. 1998). Ghosting can be affected by EEG equipment where susceptibility-related fields are responsible. Hardware improvements to increase gradient shape accuracy and reduce eddy currents, for example, or corrections to account for these inconsistencies can all reduce the artefact level (Fischer and Ladebeck 1998). One method frequently employed to correct these mismatches in alternate lines is to employ a reference scan (or navigator echo) (Hu and Le 1996; Ordidge et al. 1994b; Wan et al. 1997). The echo train used for the EPI acquisition is performed without PE gradients. A series of echoes is formed that can alternately be reversed in time. Any shift in the TE between them (in k-space) will produce a corresponding linear phase shift in image space. This allows the phase of the Fourier-transformed echoes to be compared and the difference between them used to correct all subsequent acquisitions. A further improvement can often be made to ghosting performance if the actual k-space trajectory is measured (Duyn et al. 1998; Josephs et al. 2000). One key consideration for fMRI is the stability of the ghost, because temporal changes due to drift or correction of imaging hardware can lead to false positive activation and a reduction in temporal SNR (TSNR) (see Sect. 4.1). Ghosting can still provide significant image artefacts, particularly at higher field strengths and where EEG equipment decreases magnetic field homogeneity.

2.5 RF Interference

MRI systems are specifically designed to be maximally sensitive to RF signals around a particular frequency called the Larmor frequency of the system. RF signals are highly prevalent, particularly in the typical environment of a scanner in a busy hospital or research laboratory surrounded by a wide range of electronic equipment. To record the relatively weak RF signals from the sample without any of these confounding signals from the local RF background, the magnet is placed within a Faraday cage. This is an enclosed conductive metal sheet or fine mesh that is connected to earth, and when external static or electromagnetic radiation is incident on the cage, electric currents are generated (and dissipated

via the earth) which nullify the signal within the enclosed region. To make this approach effective, a good earth and complete enclosure of a room is required. This suggests an obvious weakness of MRI systems: access in and out of the room is essential, necessitating a door; gradient and RF systems require connection through the cage. The two weak points of the Faraday cage are thus the door and filter panel. Typically, attenuation of RF to 100 dB is specified, although in practice this can be difficult to achieve. Finally, equipment for stimulus presentation, physiological monitoring, or indeed EEG equipment within the scanner room requires extra consideration. Firstly, by introducing these extra active components within the cage, any RF or electrostatic discharges they may produce will cause interference and degrade image quality. Secondly, equipment with any kind of highly conductive wire or cable crossing from outside to inside the cage (i.e. via a waveguide) is a potential route for RF to be brought into the room. A more detailed description of methods for addressing these issues is given in the chapter "EEG Instrumentation and Safety". RF interference is generally visible in one of two forms in images: an increase in the overall background noise in an image more easily quantified as a corresponding decrease in SNR, attributable to incoherent broadband RF; and/or spatially localised bright spots in the image, attributable to coherent RF at distinct frequencies, as in Fig. 8C. In most structural imaging, the RF, due to its (slice-independent) constant frequency, will appear at the same position on each slice. For EPI, this is somewhat complicated by the fact that each readout direction is reversed, resulting in the N/2 ghost of the RF artefact due to local phase inconsistencies. A repeat of the artefact in the readout direction is often produced. fMRI is particularly sensitive to RF interference because it causes a local fluctuation in the signal intensity, which can dramatically increase the temporal variance and thus severely affect sensitivity to activation. This may result in false positive activation, particularly if any of the equipment is switched on during image acquisition. We address detection and monitoring of RF performance in more detail in Sect. 5.3.

3 Other Sources of Image Artefact in fMRI

3.1 Bulk Head Motion

The recorded EEG and fMRI time series are both highly sensitive to motion. The greatest effort should be put into minimising subject movement via better head restraint and increased comfort (Laufs et al. 2008). This is especially important for patient studies in general (Hamandi et al. 2004; Salek-Haddadi et al. 2003) and when recording the highly motion-sensitive EMG. The use of a vacuum head cushion (Benar et al. 2003) has been found to minimise both motion-induced artefacts on the images and motion-induced currents contaminating the electrophysiological signal. Additionally, bite bars, inflating cuffs and subject-specific moulded cushions are also used in some centres. The use of sedative agents to suppress motion needs careful consideration, as "neuroactive" substances can alter net synaptic activity in a region-specific manner and thus fMRI signal intensity

(Kleinschmidt et al. 1999). Under certain circumstances, sedation must be considered, such as when studying very young children with fMRI (Jacobs et al. 2007).

MRI motion correction via image realignment typically entails affine coregistration, and is normally effective at dealing with small differences in head position through a scan (Ashburner and Friston 2004). However, it should be remembered that the effects of motion can last longer than the period of movement itself; for example, the effective TR seen by tissue moved into a different slice will be different, leading to signal fluctuations lasting for several TR periods (Friston et al. 1996). By including the motion realignment parameters, and preferably an expansion to take into account these extra effects, motion-related variance can be effectively modelled within general linear model (GLM) analyses (Friston et al. 1996; Lund et al. 2005). If large motion events occur, it is worth considering nulling their effects. Again, the preferred method is to include extra regressors (one for each large motion event) into the GLM to account for this variance (Lemieux et al. 2007; Salek-Haddadi et al. 2006) (as opposed to removal of data from the time series). Valuable data sets can often be recovered if motion effects are modelled sufficiently at the analysis stage (Lemieux et al. 2007). Motion correction can also be performed using navigator echoes (Ordidge et al. 1994b), which relies on the Fourier shift theorem whereby a spatial shift of the image can be detected and corrected by measurement of the phase shift within MRI k-space data.

3.2 Physiological Noise

Some "noise" is physiological and related to global or local changes in brain state that happen spontaneously. These signals were previously considered as being purely noise in terms of cognitive, paradigm-driven experiments. However, increasingly, these spontaneous changes are being treated as signals of interest (Biswal et al. 1995; Fox and Raichle 2007; Laufs et al. 2003). EEG–fMRI allows some interpretation of these spatial patterns in terms of brain state (Laufs et al. 2008), and this will be addressed in more detail in subsequent chapters.

Cardiac and respiratory cycles also can cause confounding signal changes. These occur due to motion of the whole head and from changes in pressure within the skull resulting in pulsatile motion of the brain. Due to the temporal resolution of fMRI normally being below that of the cardiac signals, aliasing occurs and must be accounted for; otherwise these effects can look like low-frequency BOLD-related signal changes. Methods are available to derive regressors from EEG/EOG/ECG signals for subsequent entry into standard GLM analysis to remove any confounding signal variance from these sources (Glover et al. 2000; Liston et al. 2006).

4 The Impact of EEG Recording on MR Image Quality

In the chapters "EEG Quality: Origin and Reduction of the EEG Cardiac-Related Artefact" and "EEG Quality: The Image Acquisition Artefact", the effects of MRI on the EEG signal were discussed; here, we instead look at the potential influence of the EEG system on MRI

image quality. As previously described, fMRI relies on good SNR, a high degree of temporal stability, and can be affected by artefacts due to the way that GE-EPI data is acquired. The presence of an EEG system can interact with both the static and rotating magnetic fields required for signal excitation and reception (Mullinger et al. 2007), which can have a subsequent impact on image quality (Krakow et al. 2000), as described below. Fortunately, these effects can be minimised by careful design of the EEG equipment.

4.1 Main Static Magnetic Field (B_0) Effects

MRI utilises a very strong, highly uniform main magnetic field, which is perturbed by the presence of any material with a magnetic susceptibility (χ). This degree of disturbance depends on the main field strength and the magnetic susceptibility ($\Delta B_0 = \chi B_0$). The high strength of the main field dictates that even weakly magnetic material such as water ($\chi = \sim 1 \times 10^{-7}$) can cause a local change in the magnetic field that can increase the distortion, dropout and ghosting described above. The main magnetic field can be readily measured from two gradient echo images with a different TE. The local difference between the phase of the images is due to the local magnetic fields, and so the offset of the field in Hz can be calculated (as for distortion correction). Even the weakly magnetic materials typically used in an MRI-compatible EEG cap have susceptibility values capable of introducing artefacts. The effect of two different commercially available MRI caps (both employing Ag/AgCl ring electrodes, 5 kΩ resistors, copper-braided wires and Abralyte 200 conductive gel) on the B_0 field in a uniform phantom taken from Mullinger et al. is shown in Fig. 5. There are clear localised regions of decreased homogeneity caused by the electrodes of the cap that are made worse with higher field strength. Taken over the volume, there is an increase in the number of pixels with a large field offset (Mullinger et al. 2007). However, in the same study, a similar measurement over the human brain at 3 T did not yield such a clear difference between cap on/cap off. A range of materials are available for the electrode heads, connecting wires, current-limiting resistors added for safety reasons (Lemieux et al. 1997), adhesives and gels, although a balance must be struck between EEG performance and the imaging requirements. Two factors determine the severity and impact of artefact caused by these components at a given field strength: its susceptibility and its position relative to both imaging and brain geometry. The relative geometry of the head and the electrodes is fixed by the experimental requirement of good EEG coverage (Debener et al. 2008). The available evidence suggests that plastic AgCl-coated electrodes can yield a small improvement in B_0 performance, although Ag/AgCl electrodes can also perform similarly in terms of image quality (Stevens et al. 2007) and may provide improved EEG quality. Both of these electrode types caused B_0 field perturbations over 10–15 mm at 4 T (Stevens et al. 2007) and so should not unduly affect signals from the brain when imaging the human head. Alternatives to the commonly used metallic EEG electrode materials (silver, silver chloride, gold) such as carbon may also yield low artefact levels (Krakow et al. 2000), while Sn or brass plated with Ni then Au can cause greater problems (Baumann and Noll 1999; Stevens et al. 2007). The susceptibility of most electrode gels is broadly similar to tissue (due to the conductivity required for EEG), giving limited scope for improvement in susceptibility-related artefacts caused by the gel/air interface. The choice of material for

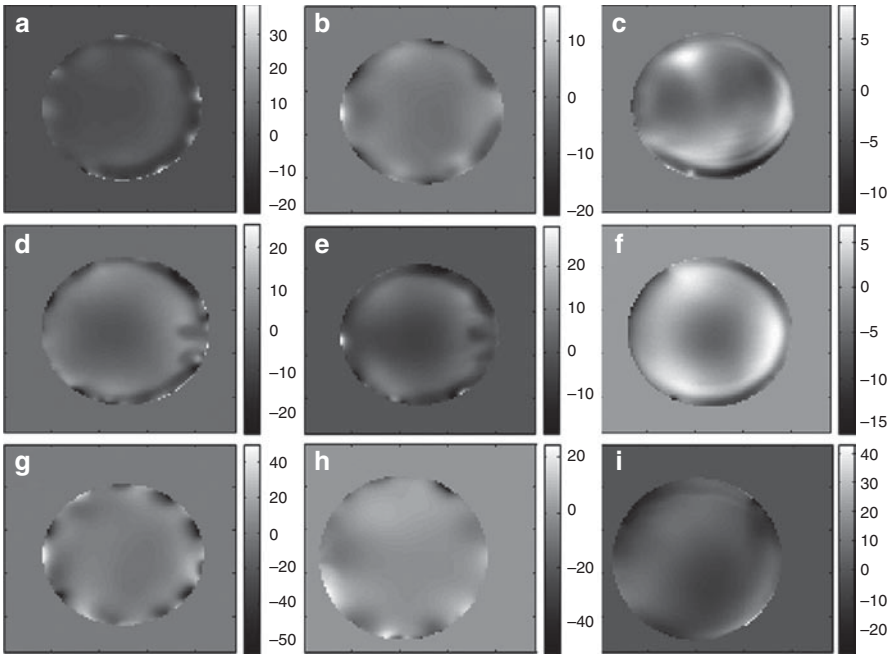

Fig. 5a–i B_0 field maps (in Hz) acquired from the phantom. Maps are shown after removal of large-scale field variations (due to the global shim) to view primarily the effect of the EEG cap at 1.5 T (**a–c**), 3 T (**d–f**) and 7 T (**g–i**) with the 64-electrode cap (*left*), 32-electrode cap (*centre*) and no cap (*right*) on. Reproduced with permission from Mullinger et al. (2007)

the safety resistors needs more careful selection, as many resistors use ferro- or diamagnetic materials, for example in the end caps connecting the terminating wires to the resistive material (Krakow et al. 2000). In the tests of Mullinger et al. (2007), the interface between the plastic surface of the phantom and the EEG electrodes and gel is likely to be the source of the greater variance in B_0. This interface is not present in the human head (see Fig. 6), where B_0 variation appears to be reduced compared to within the phantom. Increased inhomogeneity in B_0 will be seen as increased EPI image artefacts, with dropout, distortion and potentially ghosting produced. However, provided that the materials used for EEG electrodes and gel are carefully chosen and tested, there is only a small increase in B_0 inhomogeneity within the human brain, limiting the impact on image quality.

4.2 Transverse Rotational Magnetic Field (B_1) Effects

MRI signal excitation and reception uses a rotating RF field at the Larmor frequency, as described in Sect. 3.1.2. To excite the sample, an RF field is applied that causes the magnetisation to be rotated from the longitudinal axis into the transverse plane. This magnetisation then subsequently creates a rotating RF field that can then be detected by the RF coil. Any nonuniformity in the excitation profile makes it difficult to excite all of the magnetisa-

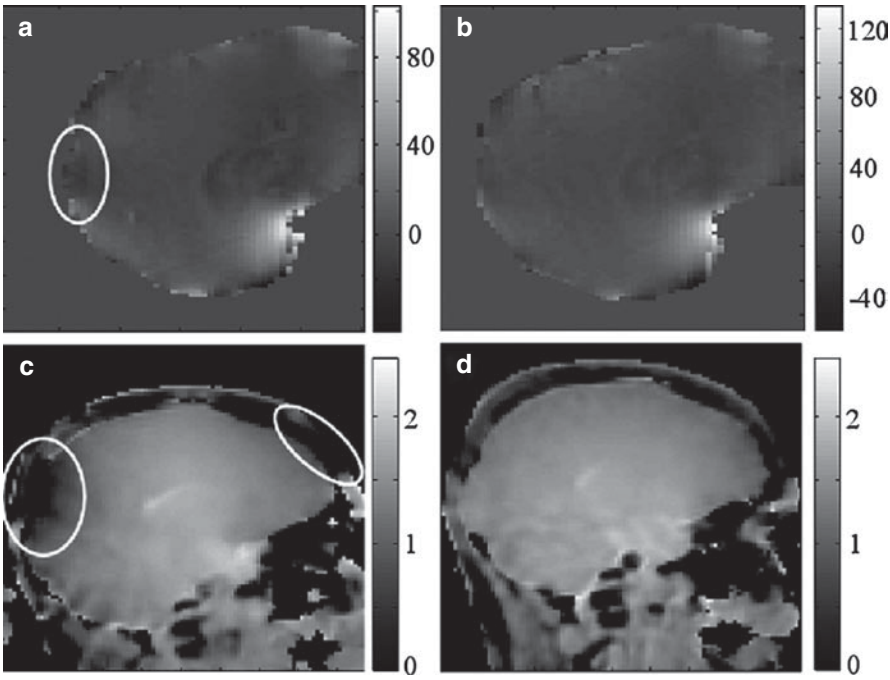

Fig. 6a–d B_0 and B_1 maps obtained in the human head. Effects of 32-electrode cap at 3 T on B_0 maps (in Hz) (**a**, **b**) and flip angle maps (normalised to average flip angle) (**c**, **d**). **a**, **c** Acquired with the cap on (regions affected are *highlighted*); **b**, **d** with no cap. Reproduced with permission from Mullinger et al (2007)

tion within the object (i.e. the flip angle will not be uniformly 90° across the object), and so some regions will suffer a corresponding signal reduction. Via the principle of reciprocity (Hoult and Lauterbur 1976), the B_1 field created by the coil for signal excitation is the same as the sensitivity of the coil (the MRI correlate of an EEG gain matrix) for signal detection. This means that the object will have a spatial variation in signal detection performance with the same pattern as for signal excitation.[2] Furthermore, the introduction of any conductive or dielectric material (i.e. the head or an EEG electrode) causes a change in the B_1 field (Sled and Pike 1998). This is because the field induces surface currents in the material that act to minimise the field produced within the object (i.e. they shield the object from the field). It is useful to consider the effects on two length scales: firstly, a global effect from the introduction of the EEG system that can generally be considered a loss of coil efficiency, and so SNR (see the section on the impact on SNR); secondly, local changes in the B_1 field are produced by local current flow which acts to reduce the B_1 field. This will produce areas with a reduced flip angle for signal excitation, and so a reduced signal and a corresponding drop in sensitivity for signal reception.

[2]This assumes that the same coil is used for both signal excitation and reception. It is increasingly common for different coils to be used for each purpose, with each imposing a different pattern.

The B_1 performance for the two EEG caps described in the previous section in a phantom can be seen in Fig. 7. The EEG cap has an effect on B_1 that appears to increase with field strength and is worse around the ECG wire. This is likely to be due to the increased

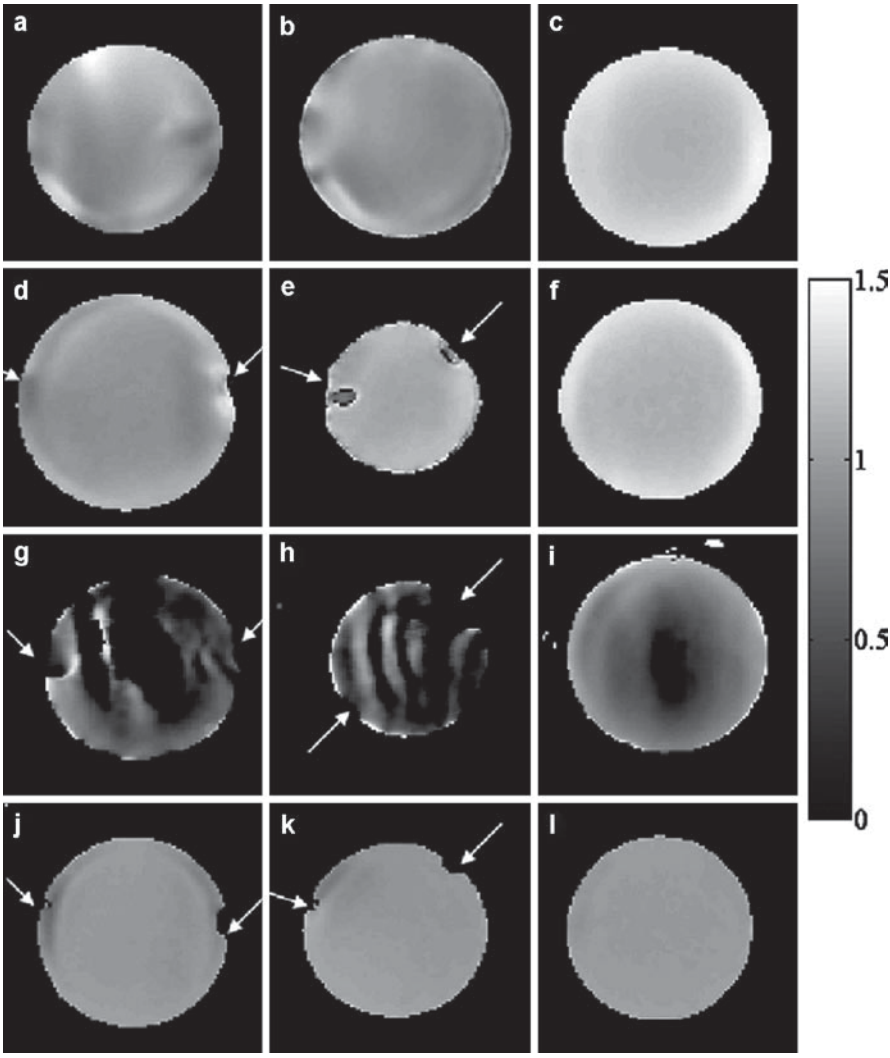

Fig. 7a–l Flip angle maps (B_1) acquired from a phantom. Flip angle maps of the phantom (normalised to average flip angle) with the 64-electrode cap (*left*), the 32-electrode cap (*centre*) and no cap (*right*). **a–c** show maps acquired at 3 T from similar slices to those shown in Fig. 1. The maps shown in the rest of the figure are taken from more inferior slices and show the effect of B_1 perturbations occurring in proximity to the ECG and EOG wires (*arrowed*) at 3 T (**d–f**), 7 T (**g–i**) and 1.5 T (**j–l**). A more inferior slice is shown for the 64-electrode cap compared with the 32-electrode cap, as the paths of the EOG and ECG wires were different on these caps. Thresholding in low-signal areas leads to the generation of significantly sized areas in the 7 T maps where the flip angle can not be characterised. Reproduced with permission from Mullinger et al (2007)

coupling of the longer length ECG wire to the RF field, with the induction of greater currents than for the shorter EEG wires. The B_1 perturbation produced by the electrodes themselves appears weak, at least at the lower field strengths. Increased electrode impedance decreases the perturbation in the B_1 field: Krakow et al. demonstrated that both plastic coated with AgCl and carbon electrodes, which offer greater impedance than metallic electrode materials, gave less artefact (Krakow et al. 2000). However, in a different comparison of electrodes at 4 T, where B_1 was independently assessed, similar shielding was produced by three different electrode types, with shielding reduced to 5% at 10–11 mm from the electrode (Stevens et al. 2007). In addition, secondary currents can flow in the safety resistors and cause artefacts, so these must be chosen carefully. Electrode wires can cause B_1 perturbations, even when safety resistors are present (Mullinger et al. 2007); higher-impedance alternatives such as carbon can reduce this artefact (Krakow et al. 2000).

RF pulses that aim to produce a uniform flip angle despite local variation in B_1 (frequently referred to as "adiabatic" pulses) do exist (Garwood et al. 1989; Garwood and Delabarre 2001), but are more commonly employed for global signal inversion or refocusing, and normally require greater RF power than standard excitation pulses (de Graaf et al. 1996). Certainly, investigation of EEG–fMRI performance with spatially selective 90° pulses that exhibit acceptable off-resonance behaviour such as derivatives of the BIR4 pulse (de Graaf et al. 1996; Shen and Rothman 1997) are merited, and may be essential to limit artefacts at higher field strengths. B_1 perturbations will produce regional intensity variation in EPI images without increased distortion. One simple method to determine whether B_1 or B_0 field effects are responsible for regionally reduced performance (where B_0 and B_1 mapping sequences are not available) is to compare spin echo 2DFT images with the EPI; where both exhibit changes in image intensity, the problem can be assigned to a local B_1 effect.

4.3 Impact on SNR

The overall effect of the introduction of the EEG system is a reduction in SNR. Locally this can be due to reduced signal related to decreased B_0 and B_1 homogeneity. Globally, there will be an average reduction in B_1 sensitivity due to the introduction of EEG equipment from shielding effects, and increased noise from increased RF coil impedance, with a concomitant global reduction in SNR. The shielding effect is a reduction in B_1 in the head from induced current flow in the EEG electrodes. To understand the increase in noise, the system can be considered as a whole with a highly resonant RF coil circuit having its impedance increased by the introduction of the head, and then further increased by the introduction of EEG components. While the increase in impedance (a reduction in the coil efficiency usually measured by the Q factor) is one effect, it is also possible that the whole system (coil with head and EEG system inside) suffers from a split or shifted resonant frequency. In this case, a quite dramatic reduction in coil performance can result. A reduction in SNR within the images will be seen, but, where the same coil is used for RF transmission, there will also be a large increase in the transmitted power required for a particular RF excitation, and increased local electric fields with the associated safety risks (Lemieux et al. 1997).

In the image quality study of Krakow et al. (2000), only the increase in electronic noise due to the introduction of the EEG amplifier was investigated, and no noise increase was detected when properly shielded. While this approach will detect any RF interference, it does not determine the amount of SNR loss due to a reduction in the RF coil performance via the mechanisms described above. One previous study observed a reduction in SNR that was proportional to the number of electrodes in the cap (Scarff et al. 2004), while an innovative ink cap that uses conductive ink rather than conventional wires had little apparent effect on the SNR (Vasios et al. 2006). More recently, tests of two commercially available caps at different field strengths on five subjects found a reduction of 4–28% in the TSNR. A smaller SNR reduction was found on the 3 T system, although this could be due to cap design and may not lead to a large difference in detected activation (Bonmassar et al. 2001). While some decrease in TSNR (see Sect. 5.1) could be caused by increased movement due to the greater discomfort of wearing an EEG cap, it is likely that this is also because of cap–coil interaction. It is worth noting that reducing the appearance of B_1-related artefacts is worthwhile even when they do not appear to greatly affect signal from the brain, because reducing this interaction will improve the overall SNR performance via reduced loading/detuning of the RF coil.

5 fMRI Quality Assurance (QA)

The large demands placed on MRI hardware by scanning at close to the maximum gradient switching rate and amplitude for extended periods, coupled with the sensitivity of fMRI to any temporal signal changes, means that careful, regular fMRI QA is important to ensure that scanner performance is maximised and any faults are quickly detected. In this section, some of the key QA measurements are described. In many respects, the principle is more important than any specific tests; the more that careful, regular, quantitative monitoring of the system is performed, the better. In particular, we focus on tests aimed more generally at fMRI QA, but which constitute a good basic set of tests of fMRI data quality that can be performed both with and without the EEG equipment. A summary of this can be found in Table 1.

5.1 Quantification of SNR and Temporal SNR

The receiver bandwidth determines the frequencies and levels of signal and noise obtained (given a certain object imaged at a specified resolution), since most of the signal is normally concentrated at low frequencies, whereas the noise is distributed across the frequency range. However, given that a certain bandwidth is used for a specific scan protocol, then the SNR describes the quality of the data and can be very sensitive, if nonspecific, to the performance of most components of the system. A phantom should be used that

Table 1 Examples of QA procedures

Scans	Suggested frequency	Example parameters	Example measurements	What to look out for	Possible cause
Spin echo 2DFT	Daily	192×128 matrix, TE = minimum, TR = 3 s, 5 central slices	SNR	Change or fluctuations in value	Nonspecific
EPI (as used for EEG–fMRI)	Weekly	TR = 2000 ms, TE = 30 ms, 200 volumes, 27 slices	Temporal mean	Strong repeats of the image (ghosts)	Gradient performance, timing and pre-emphasis, phase correction errors
			Temporal SD reformatted as coronal sections	Lines in the slice direction / strong images	RF interference / B0 and possible gradient drift
			Weisskoff plot	Change in plot	Nonspecific
			RDC	Change in value	Nonspecific
EPI (as used for EEG–fMRI) with and without EEG cap	Monthly	TR = 2000 ms, TE = 30 ms, 200 volumes, 27 slices		Compare with the measurements without EEG equipment	EEG system fault
Repeat run	Monthly	Place slices outside the phantom and set the transmit gain to zero. Run for >10 min, i.e. 400 volumes	Play the images back as a movie with a volume in each frame	Changes in background noise level, any structure in the noise	Coherent noise patterns within certain slices suggests spiking from the gradients or electrostatic discharges from another source. Higher signal in a consistent spatial position indicates RF interference

approximates the size and loading (RF interaction) of the human head. A phantom made of gel to eliminate flow effects is also desirable for testing fMRI temporal stability. Highly accurate and easily reproducible positioning of the phantom is important within both the RF coil and the main magnetic field isocentres (i.e. the SNR measured should not change when the test is performed by a different person!). Where different RF coils are routinely employed, each should be regularly tested. Different methods can be used to take a measurement of the signal and noise. However, most simple SNR tests (such as those described here) make the assumptions that the background noise follows a Raleigh distribution in the magnitude image and that the spatial distribution of noise is homogeneous. These criteria are not met in most images from array receiver coils, or where image filtering or corrections have been applied (Constantinides et al. 1997; Dietrich et al. 2007). To sample the signal, an image of the object must be obtained and the average signal within it calculated, typically by averaging the signal over a large (>75%) area. Noise can be measured in a

similar manner by taking several background regions in the image and averaging them, although care must be taken to avoid regions exhibiting any artefact from the object, such as Gibbs ringing (Haacke et al. 1999), ghosting, or if any correction or filter is applied. An alternative approach to measure the noise is to obtain a further image using identical parameters, take the difference, and calculate the standard deviation within the same region of interest (ROI) (i.e. the area defined on the first image for the signal). This method can be affected by any temporal instability and, as such, is usefully viewed to detect any structure in the noise; if edges are visible, centre frequency or gradient drift may be indicated, or if a low SNR version of the object is apparent, RF/receiver instabilities can be responsible. Also, the value obtained from each SNR measurement method will be different by a constant factor due to the rectification of Gaussian noise when a background noise region is used. Different sequences may be employed for SNR calculation, but a fully relaxed 2DFT spin echo sequence is a highly reliable method, and is complimentary to an fMRI-specific EPI run. While standard SNR measurement is sensitive to many aspects of scanner performance, it does not generally test temporal fluctuations that can affect fMRI. In contrast to the static SNR, the TSNR includes contributions from fluctuations from scanner drift from the gradients as they heat, and from the main magnetic field, ghost fluctuations due to timing errors, etc. The TSNR is simply the mean signal in a voxel divided by its variance over time. This measure of SNR can be more reliable where PI reconstruction methods and/or image filters are applied (Dietrich et al. 2007). A number of values in addition to the TSNR can be calculated and monitored from an EPI time series obtained from a phantom. One such standardised set of measurements (used by the FBIRN consortium) that can be automated is freely available (http://www.nbirn.net) and well described (Friedman and Glover 2006). These standardised QA measurements are important for cross-centre comparison (Friedman et al. 2007).

5.2 The Weisskoff Test

The Weisskoff test is a simple method for assessing scanner stability (Weisskoff 1996) and is included within the FBIRN procedure (Friedman and Glover 2006). In its original formulation, two ROIs are obtained inside and outside the phantom for each point in time and compared as the region is linearly changed in size. Taking the average mean and standard deviation produced, the standard deviation should be reduced with the square root of number of voxels in the ROI if purely Johnson noise is present from the scanner hardware and sample. The calculation can then be repeated only where the relative fluctuation from time point to time point is calculated again as the regions are linearly changed in size. Any difference between the two curves generated is attributable to extra temporal fluctuations in the images from scanner instabilities. The performance of the scanner can thus be characterised for a particular phantom and scanning sequence and the performance assessed over time. A derivative single value measure can also be obtained from this test called the radius of decorrelation (RDC), which can be thought of as being the point at which statistical independence between voxels is lost; practically speaking, it is where the two curves described above begin to deviate (see Fig. 8).

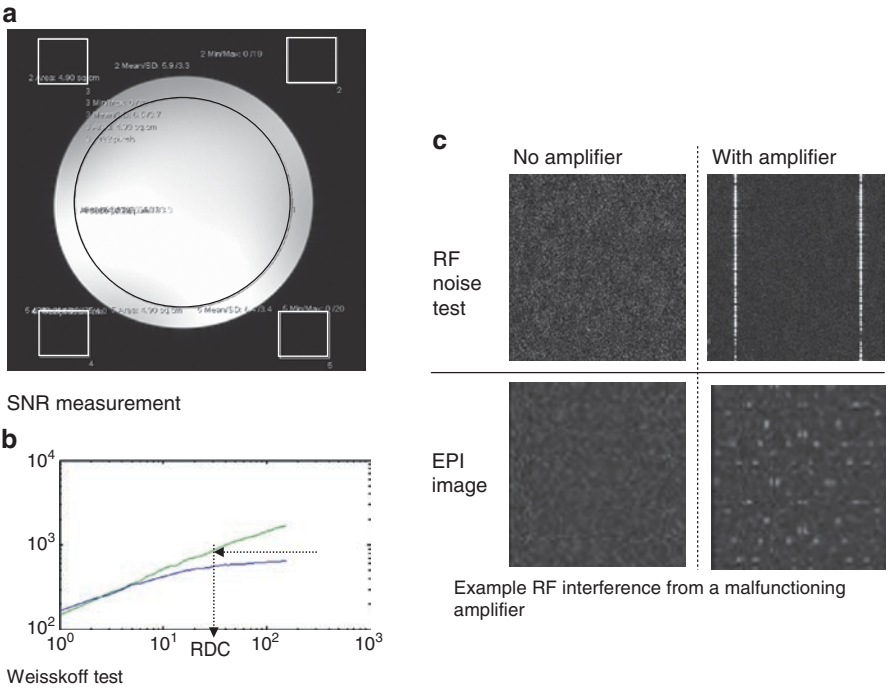

Fig. 8a–c Examples of QA measurements. An example SNR measurement is shown (**a**) with the mean and standard deviation in the regions of the signal and noise compared. An example Weisskoff plot is shown (**b**), including the radius of decorrelation. Finally, an example of the appearance of RF noise in images obtained with the RF transmitter effectively turned off is shown (**c**)

5.3 Coherent Noise Testing

While RF interference can affect other measurements such as SNR and the RDC, specific testing is useful because the introduction of EEG equipment into the scanner environment increases the potential for this problem to occur. As an additional test to those suggested above, viewing a 3D volume of the temporal variance (e.g. taking the magnitude image time series and calculating the temporal standard deviation for each voxel) is highly instructive. With the data displayed such that the slice direction is in the image plane (e.g. axial images reformatted as coronal sections), RF interference will be seen as stripes running along the slice direction because the source of the signal is the same frequency independent of the RF or imaging gradients and so it will appear in the same place. Very few other artefacts have a similar appearance (apart from possibly some flow effects). Another useful and simple test for detecting noise changes is to simply scan while not receiving signal from the object. This is normally achieved by setting the RF transmit gain to zero, and/or from imaging slices outside the object, and often requires any automated prescanning to be skipped or performed manually (because most clinical scanners will detect that no signal is present

and the centre frequency setting, for example, will fail). By looking at a long time series of images containing pure noise, any transient increases or changes in time due to RF interference or electrostatic discharges (often called spike noise) can be relatively easily detected visually. Finally, the equipment should be tested in all possible states. For example, where different gain settings, sampling frequencies or numbers of channels may be used in an EEG amplifier, it is worthwhile checking each operational state because RF noise might be generated or its frequency shifted in one particular configuration. An example of RF noise from a malfunctioning EEG amplifier is shown in Fig. 8.

6 Summary and Conclusions

Image quality is at the core of any successful investigation of brain activity using fMRI. Therefore, it is crucial to understand the mechanisms of the image formation process and its possible pitfalls, particularly when special equipment is in the vicinity of the MRI instrument, such as that used for EEG recording. In general, properly designed and tested EEG equipment should not adversely degrade image quality. The optimisation of fMRI sequences and the application of rigorous QA protocols will ensure optimal image acquisition and minimise the risks of false-negative or false-positive findings.

Acknowledgements I would like to thank the following contributors to this chapter: Ralf Deichmann (Brain Imaging Centre, Frankfurt) for his useful comments about EPI artefacts; Jack Wells (Department for Medical Physics, UCL, London), Philip Allen (Department of Clinical Neurophysiology, National Hospital for Neurology and Neurosurgery, London) and Nikolaus Weiskopf for careful reading of the manuscript; Chloe Hutton and Nikolaus Weiskopf (Wellcome Trust Centre for Neuroimaging, UCL, London) for providing the distortion correction part of Fig. 3 and the Weisskoff plot script for Fig. 8b; Alison Duncan (AMRIG, UCL, London) for providing Fig. a; Richard Bowtell (Sir Peter Mansfield Magnetic Resonance Centre, Nottingham, UK) and the International Journal of Psychophysiology (doi:10.1016/j.ijpsycho.2007.06.008) for allowing the reproduction of Figs. 5–7.

References

Ahn CB, Kim JH, Cho ZH (1986) High speed spiral scan echo planar imaging. IEEE Trans Med Imaging 5(1):2–5

Ashburner J, Friston K (2004) Rigid body registration. In: Frackowiak RSJ, Friston KJ, Frith CD, Dolan RJ, Price CJ, Zeki S, Ashburner J, Penny W (eds) Human brain function. Elsevier, Amsterdam, pp 635–653

Bandettini PA, Wong EC, Jesmanowicz A, Hinks RS, Hyde JS (1994) Spin-echo and gradient-echo EPI of human brain activation using BOLD contrast: a comparative study at 1.5 T. NMR Biomed 7:12–20

Baumann SB, Noll DC (1999) A modified electrode cap for EEG recordings in MRI scanners. Clin Neurophysiol 110:2189–2193

Benar C, Aghakhani Y, Wang Y, Izenberg A, Al Asmi A, Dubeau F, Gotman J (2003) Quality of EEG in simultaneous EEG–fMRI for epilepsy. Clin Neurophysiol 114:569–580
Biswal B, Yetkin FZ, Haughton VM, Hyde JS (1995) Functional connectivity in the motor cortex of resting human brain using echo-planar MRI. Magn Reson Med 34:537–541
Block KT, Frahm J (2005) Spiral imaging: a critical appraisal. J Magn Reson Imaging 21:657–668
Bonmassar G, Hadjikhani N, Ives JR, Hinton D, Belliveau JW (2001) Influence of EEG electrodes on the BOLD fMRI signal. Hum Brain Mapp 14:108–115
Bornert P, Jensen D (1994) Single-shot-double-echo EPI. Magn Reson Imaging 12:1033–1038
Butts K, Riederer SJ, Ehman RL, Thompson RM, Jack CR (1994) Interleaved echo planar imaging on a standard MRI system. Magn Reson Med 31:67–72
Carlson JW, Minemura T (1993) Imaging time reduction through multiple receiver coil data acquisition and image reconstruction. Magn Reson Med 29:681–687
Carmichael DW, Priest AN, De Vita E, Ordidge RJ (2005) Common SENSE (sensitivity encoding using hardware common to all MR scanners): a new method for single-shot segmented echo planar imaging. Magn Reson Med 54:402–410
Chen NK, Wyrwicz AM (1999) Correction for EPI distortions using multi-echo gradient-echo imaging. Magn Reson Med 41:1206–1213
Cho ZH, Kim DJ, Kim YK (1988) Total inhomogeneity correction including chemical shifts and susceptibility by view angle tilting. Med Phys 15:7–11
Cohen MS, Weisskoff RM, Rzedzian RR, Kantor HL (1990) Sensory stimulation by time-varying magnetic fields. Magn Reson Med 14:409–414
Constable RT, Spencer DD (1999) Composite image formation in z-shimmed functional MR imaging. Magn Reson Med 42:110–117
Constantinides CD, Atalar E, McVeigh ER (1997) Signal-to-noise measurements in magnitude images from NMR phased arrays. Magn Reson Med 38:852–857
Cusack R, Russell B, Cox SM, De Panfilis C, Schwarzbauer C, Ansorge R (2005) An evaluation of the use of passive shimming to improve frontal sensitivity in fMRI. Neuroimage 24:82–91
de Graaf RA, Nicolay K, Garwood M (1996) Single-shot, B1-insensitive slice selection with a gradient-modulated adiabatic pulse, BISS-8. Magn Reson Med 35:652–657
Debener S, Mullinger KJ, Niazy RK, Bowtell RW (2008) Properties of the ballistocardiogram artefact as revealed by EEG recordings at 1.5, 3 and 7 T static magnetic field strength. Int J Psychophysiol 67:189–199
Deichmann R, Gottfried JA, Hutton C, Turner R (2003) Optimized EPI for fMRI studies of the orbitofrontal cortex. Neuroimage 19:430–441
Deichmann R, Josephs O, Hutton C, Corfield DR, Turner R (2002) Compensation of susceptibility-induced BOLD sensitivity losses in echo-planar fMRI imaging. Neuroimage 15:120–135
Dietrich O, Raya JG, Reeder SB, Reiser MF, Schoenberg SO (2007) Measurement of signal-to-noise ratios in MR images: influence of multichannel coils, parallel imaging, and reconstruction filters. J Magn Reson Imaging 26:375–385
Duong TQ, Yacoub E, Adriany G, Hu X, Ugurbil K, Vaughan JT, Merkle H, Kim SG (2002) High-resolution, spin-echo BOLD, and CBF fMRI at 4 and 7 T. Magn Reson Med 48:589–593
Duyn JH, Yang Y, Frank JA, van der Veen JW (1998) Simple correction method for k-space trajectory deviations in MRI. J Magn Reson 132:150–153
Feinberg DA, Hale JD, Watts JC, Kaufman L, Mark A (1986) Halving MR imaging time by conjugation: demonstration at 3.5 kG. Radiology 161:527–531
Feinberg DA, Kiefer B, Johnson G (1995) GRASE improves spatial resolution in single shot imaging. Magn Reson Med 33:529–533
Feinberg DA, Oshio K (1994) Phase errors in multi-shot echo planar imaging. Magn Reson Med 32:535–539
Feinberg DA, Reese TG, Wedeen VJ (2002) Simultaneous echo refocusing in EPI. Magn Reson Med 48:1–5

Fernandez-Seara MA, Wang Z, Wang J, Rao HY, Guenther M, Feinberg DA, Detre JA (2005) Continuous arterial spin labeling perfusion measurements using single shot 3D GRASE at 3 T. Magn Reson Med 54:1241–1247
Fischer H, Ladebeck R (1998) Echo-planar imaging image artefacts. In: Schmitt F, Stehling MK, Turner R (eds) Echo-planar imaging. Springer, Berlin, pp 180–200
Fox MD, Raichle ME (2007) Spontaneous fluctuations in brain activity observed with functional magnetic resonance imaging. Nat Rev Neurosci 8:700–711
Frahm J, Merboldt KD, Hanicke W (1993) Functional MRI of human brain activation at high spatial resolution. Magn Reson Med 29:139–144
Frahm J, Merboldt KD, Hanicke W (1988) Direct FLASH MR imaging of magnetic field inhomogeneities by gradient compensation. Magn Reson Med 6:474–480
Friedman L, Glover GH (2006) Report on a multicenter fMRI quality assurance protocol. J Magn Reson Imaging 23:827–839
Friedman L, Stern H, Brown GG, Mathalon DH, Turner J, Glover GH, Gollub RL, Lauriello J, Lim KO, Cannon T, Greve DN, Bockholt HJ, Belger A, Mueller B, Doty MJ, He J, Wells W, Smyth P, Pieper S, Kim S, Kubicki M, Vangel M, Potkin SG (2007) Test-retest and between-site reliability in a multicenter fMRI study. Hum Brain Mapp 29:958–972
Friston KJ, Williams S, Howard R, Frackowiak RS, Turner R (1996) Movement-related effects in fMRI time-series. Magn Reson Med 35:346–355
Garwood M, Delabarre L (2001) The return of the frequency sweep: designing adiabatic pulses for contemporary NMR. J Magn Reson 153:155–177
Garwood M, Ugurbil K, Rath AR, Bendall MR, Ross BD, Mitchell SL, Merkle H (1989) Magnetic resonance imaging with adiabatic pulses using a single surface coil for RF transmission and signal detection. Magn Reson Med 9:25–34
Glover GH, Law CS (2001) Spiral-in/out BOLD fMRI for increased SNR and reduced susceptibility artifacts. Magn Reson Med 46:515–522
Glover GH, Li TQ, Ress D (2000) Image-based method for retrospective correction of physiological motion effects in fMRI: RETROICOR. Magn Reson Med 44:162–167
Griswold MA, Jakob PM, Heidemann RM, Nittka M, Jellus V, Wang J, Kiefer B, Haase A (2002) Generalized autocalibrating partially parallel acquisitions (GRAPPA) 121. Magn Reson Med 47:1202–1210
Gruetter R (1993) Automatic, localized in vivo adjustment of all first- and second-order shim coils. Magn Reson Med 29:804–811
Gruetter R, Tkac I (2000) Field mapping without reference scan using asymmetric echo-planar techniques. Magn Reson Med 43:319–323
Haacke EM, Brown RW, Thompson MR, Venkatesan R (1999) The continuous and discrete Fourier transforms. In: Magnetic resonance imaging: physical principles and sequence design. Wiley, New York, pp 207–230
Hamandi K, Salek-Haddadi A, Fish DR, Lemieux L (2004) EEG/functional MRI in epilepsy: the Queen Square Experience. J Clin Neurophysiol 21:241–248
Hennel F, Nedelec JF (1995) Interleaved asymmetric echo-planar imaging. Magn Reson Med 34:520–524
Hoult DI, Lauterbur PC (1976) The signal to noise ratio of the nuclear magnetic resonance experiment. J Magn Reson 34:425–433
Hu X, Le TH (1996) Artifact reduction in EPI with phase-encoded reference scan. Magn Reson Med 36:166–171
Hutchinson M, Raff U (1988) Fast MRI data acquisition using multiple detectors. Magn Reson Med 6:87–91
Hutton C, Bork A, Josephs O, Deichmann R, Ashburner J, Turner R (2002) Image distortion correction in fMRI: a quantitative evaluation. Neuroimage 16:217–240

Jacobs J, Kobayashi E, Boor R, Muhle H, Stephan W, Hawco C, Dubeau F, Jansen O, Stephani U, Gotman J, Siniatchkin M (2007) Hemodynamic responses to interictal epileptiform discharges in children with symptomatic epilepsy. Epilepsia 48:2068–2078

Jezzard P, Balaban RS (1995) Correction for geometric distortion in echo planar images from B0 field variations 50. Magn Reson Med 34:65–73

Jezzard P, Clare S (1999) Sources of distortion in functional MRI data. Hum Brain Mapp 8:80–85

Josephs O, Weiskopf N, Deichmann R, Turner R (2000) Trajectory measurement and generalised reconstruction in rectilinear EPI. In: Proc 8th Int Meet ISMRM, Denver, CO, USA, 1–7 April 2000

Kleinschmidt A, Bruhn H, Kruger G, Merboldt KD, Stoppe G, Frahm J (1999) Effects of sedation, stimulation, and placebo on cerebral blood oxygenation: a magnetic resonance neuroimaging study of psychotropic drug action. NMR Biomed 12:286–292

Krakow K, Allen PJ, Symms MR, Lemieux L, Josephs O, Fish DR (2000) EEG recording during fMRI experiments: image quality. Hum Brain Mapp 10:10–15

Lamberton F, Delcroix N, Grenier D, Mazoyer B, Joliot M (2007) A new EPI-based dynamic field mapping method: application to retrospective geometrical distortion corrections. J Magn Reson Imaging 26:747–755

Laufs H, Daunizeau J, Carmichael DW, Kleinschmidt A (2008) Recent advances in recording electrophysiological data simultaneously with magnetic resonance imaging. Neuroimage 40:515–528

Laufs H, Krakow K, Sterzer P, Eger E, Beyerle A, Salek-Haddadi A, Kleinschmidt A (2003) Electroencephalographic signatures of attentional and cognitive default modes in spontaneous brain activity fluctuations at rest. Proc Natl Acad Sci USA 100:11053–11058

Lemieux L, Allen PJ, Franconi F, Symms MR, Fish DR (1997) Recording of EEG during fMRI experiments: patient safety. Magn Reson Med 38:943–952

Lemieux L, Salek-Haddadi A, Lund TE, Laufs H, Carmichael D (2007) Modelling large motion events in fMRI studies of patients with epilepsy. Magn Reson Imaging 25:894–901

Liston AD, Lund TE, Salek-Haddadi A, Hamandi K, Friston KJ, Lemieux L (2006) Modelling cardiac signal as a confound in EEG–fMRI and its application in focal epilepsy studies. Neuroimage 30:827–834

Lund TE, Norgaard MD, Rostrup E, Rowe JB, Paulson OB (2005) Motion or activity: their role in intra- and inter-subject variation in fMRI. Neuroimage 26:960–964

Lutcke H, Merboldt KD, Frahm J (2006) The cost of parallel imaging in functional MRI of the human brain. Magn Reson Imaging 24:1–5

Mackenzie IS, Robinson EM, Wells AN, Wood B (1987) A simple field map for shimming. Magn Reson Med 5:262–268

Mansfield P (1977) Multi-planar image formation using NMR spin echoes. J Phys C 10:L55–L58

Mansfield P (1984) Spatial mapping of the chemical shift in NMR. Magn Reson Med 1:370–386

Mansfield P, Harvey PR (1993) Limits to neural stimulation in echo-planar imaging. Magn Reson Med 29:746–758

Menon RS, Thomas CG, Gati JS (1997) Investigation of BOLD contrast in fMRI using multi-shot EPI. NMR Biomed 10:179–182

Merboldt KD, Finsterbusch J, Frahm J (2000) Reducing inhomogeneity artifacts in functional MRI of human brain activation-thin sections vs gradient compensation. J Magn Reson 145: 184–191

Miller KL, Hargreaves BA, Lee J, Ress D, deCharms RC, Pauly JM (2003) Functional brain imaging using a blood oxygenation sensitive steady state. Magn Reson Med 50:675–683

Miller KL, Hargreaves BA, Lee J, Ress D, deCharms RC, Pauly JM (2004) Functional brain imaging with BOSS FMRI. Conf Proc IEEE Eng Med Biol Soc 7:5234–5237

Miller KL, Smith SM, Jezzard P, Pauly JM (2006) High-resolution FMRI at 1.5T using balanced SSFP. Magn Reson Med 55:161–170
Morgan PS, Bowtell RW, McIntyre DJ, Worthington BS (2004) Correction of spatial distortion in EPI due to inhomogeneous static magnetic fields using the reversed gradient method. J Magn Reson Imaging 19:499–507
Mullinger K, Debener S, Coxon R, Bowtell R (2007) Effects of simultaneous EEG recording on MRI data quality at 1.5, 3 and 7 tesla. Int J Psychophysiol 67:178–188
Munger P, Crelier GR, Peters TM, Pike GB (2000) An inverse problem approach to the correction of distortion in EPI images. IEEE Trans Med Imaging 19:681–689
Nair G, Duong TQ (2004) Echo-planar BOLD fMRI of mice on a narrow-bore 9.4 T magnet. Magn Reson Med 52:430–434
Norris DG, Zysset S, Mildner T, Wiggins CJ (2002) An investigation of the value of spin-echo-based fMRI using a Stroop color-word matching task and EPI at 3 T. Neuroimage 15:719–726
Ordidge R (1999) The development of echo-planar imaging (EPI): 1977–1982. MAGMA 9;117–121
Ordidge RJ, Gorell JM, Deniau JC, Knight RA, Helpern JA (1994a) Assessment of relative brain iron concentrations using T2-weighted and T2*-weighted MRI at 3 Tesla. Magn Reson Med 32:335–341
Ordidge RJ, Helpern JA, Qing ZX, Knight RA, Nagesh V (1994b) Correction of motional artifacts in diffusion-weighted MR images using navigator echoes. Magn Reson Imaging 12:455–460
Parkes LM, Schwarzbach JV, Bouts AA, Deckers RH, Pullens P, Kerskens CM, Norris DG (2005) Quantifying the spatial resolution of the gradient echo and spin echo BOLD response at 3 Tesla. Magn Reson Med 54:1465–1472
Poser BA, Versluis MJ, Hoogduin JM, Norris DG (2006) BOLD contrast sensitivity enhancement and artifact reduction with multiecho EPI: parallel-acquired inhomogeneity-desensitized fMRI. Magn Reson Med 55:1227–1235
Preston AR, Thomason ME, Ochsner KN, Cooper JC, Glover GH (2004) Comparison of spiral-in/out and spiral-out BOLD fMRI at 1.5 and 3 T. Neuroimage 21:291–301
Priest AN, Carmichael DW, De Vita E, Ordidge RJ (2004) Method for spatially interleaving two images to halve EPI readout times: two reduced acquisitions interleaved (TRAIL) Magn Reson Med 51:1212–1222
Priest AN, De Vita E, Thomas DL, Ordidge RJ (2006) EPI distortion correction from a simultaneously acquired distortion map using TRAIL. J Magn Reson Imaging 23:597–603
Pruessmann KP, Weiger M, Scheidegger MB, Boesiger P (1999) SENSE: sensitivity encoding for fast MRI 18. Magn Reson Med 42;952–962
Reber PJ, Wong EC, Buxton RB, Frank LR (1998) Correction of off resonance-related distortion in echo-planar imaging using EPI-based field maps. Magn Reson Med 39:328–330
Reeder SB, Atalar E, Bolster BD Jr, McVeigh ER (1997) Quantification and reduction of ghosting artifacts in interleaved echo-planar imaging. Magn Reson Med 38:429–439
Rzedzian R (1987) High speed, high resolution, spin echo imaging by mosaic scan and MESH. In: Proc 6th Annu Meet SMRM, New York, 17–21 Aug 1987
Salek-Haddadi A, Diehl B, Hamandi K, Merschhemke M, Liston A, Friston K, Duncan JS, Fish DR, Lemieux L (2006) Hemodynamic correlates of epileptiform discharges: an EEG–fMRI study of 63 patients with focal epilepsy. Brain Res 1088:148–166
Salek-Haddadi A, Lemieux L, Merschhemke M, Diehl B, Allen PJ, Fish DR (2003) EEG quality during simultaneous functional MRI of interictal epileptiform discharges. Magn Reson Imaging 21:1159–1166
Sangill R, Wallentin M, Ostergaard L, Vestergaard-Poulsen P (2006) The impact of susceptibility gradients on cartesian and spiral EPI for BOLD fMRI. MAGMA 19:105–114
Scarff CJ, Reynolds A, Goodyear BG, Ponton CW, Dort JC, Eggermont JJ (2004) Simultaneous 3-T fMRI and high-density recording of human auditory evoked potentials. Neuroimage 23:1129–1142

Schmidt CF, Boesiger P, Ishai A (2005) Comparison of fMRI activation as measured with gradient- and spin-echo EPI during visual perception. Neuroimage 26:852–859
Schmithorst VJ, Dardzinski BJ, Holland SK (2001) Simultaneous correction of ghost and geometric distortion artifacts in EPI using a multiecho reference scan. IEEE Trans Med Imaging 20:535–539
Schmitt F, Stehling MK, Turner R (eds) (1998) Echo-planar imaging. Springer, Berlin
Shen J, Rothman DL (1997) Adiabatic slice-selective excitation for surface coils. J Magn Reson 124:72–79
Sled JG, Pike GB (1998) Standing-wave and RF penetration artifacts caused by elliptic geometry: an electrodynamic analysis of MRI. IEEE Trans Med Imaging 17:653–662
Sodickson DK, Manning WJ (1997) Simultaneous acquisition of spatial harmonics (SMASH): fast imaging with radiofrequency coil arrays. Magn Reson Med 38:591–603
Stevens TK, Ives JR, Klassen LM, Bartha R (2007) MR compatibility of EEG scalp electrodes at 4 Tesla. J Magn Reson Imaging 25:872–877
Turner R, Ordidge RJ (2000) Technical challenges of functional magnetic resonance imaging. IEEE Eng Med Biol Mag 19:42–54
van Gelderen P, de Zwart JA, Starewicz P, Hinks RS, Duyn JH (2007) Real-time shimming to compensate for respiration-induced B0 fluctuations. Magn Reson Med 57:362–368
Vasios CE, Angelone LM, Purdon PL, Ahveninen J, Belliveau JW, Bonmassar G (2006) EEG/(f) MRI measurements at 7 Tesla using a new EEG cap ("InkCap"). Neuroimage 33:1082–1092
Wan X, Gullberg GT, Parker DL, Zeng GL (1997) Reduction of geometric and intensity distortions in echo-planar imaging using a multireference scan. Magn Reson Med 37:932–942
Ward HA, Riederer SJ, Jack CR Jr. (2002) Real-time autoshimming for echo planar timecourse imaging. Magn Reson Med 48:771–780
Weiskopf N, Hutton C, Josephs O, Deichmann R (2006) Optimal EPI parameters for reduction of susceptibility-induced BOLD sensitivity losses: a whole-brain analysis at 3 T and 1.5 T. Neuroimage 33:493–504
Weiskopf N, Hutton C, Josephs O, Turner R, Deichmann R (2007) Optimized EPI for fMRI studies of the orbitofrontal cortex: compensation of susceptibility-induced gradients in the readout direction. MAGMA 20:39–49
Weiskopf N, Klose U, Birbaumer N, Mathiak K (2005) Single-shot compensation of image distortions and BOLD contrast optimization using multi-echo EPI for real-time fMRI. Neuroimage 24:1068–1079
Weisskoff RM (1996) Simple measurement of scanner stability for functional NMR imaging of activation in the brain. Magn Reson Med 36:643–645
Wielopolski PA, Schmitt F, Stehling MK (1998) Echo-planar pulse sequences. In: Schmitt F, Stehling MK, Turner R (eds) Echo-planar imaging. Springer, Berlin, pp 65–134
Wilson JL, Jenkinson M, Jezzard P (2003) Protocol to determine the optimal intraoral passive shim for minimisation of susceptibility artifact in human inferior frontal cortex 3. Neuroimage 19:1802–1811
Wilson JL, Jezzard P (2003) Utilization of an intra-oral diamagnetic passive shim in functional MRI of the inferior frontal cortex. Magn Reson Med 50:1089–1094
Zaitsev M, Hennig J, Speck O (2004) Point spread function mapping with parallel imaging techniques and high acceleration factors: fast, robust, and flexible method for echo-planar imaging distortion correction. Magn Reson Med 52:1156–1166
Zhong K, Leupold J, Hennig J, Speck O (2007) Systematic investigation of balanced steady-state free precession for functional MRI in the human visual cortex at 3 Tesla. Magn Reson Med 57:67–73